ACS OMEGA

http://pubs.acs.org/journal/acsodf

Article

Catalytic Effect of Ferrocenyl Energetic Catalysts for *N*-Guanylurea Dinitramide (GUDN or FOX-12) Decomposition

Liping Jiang, Xiaolong Fu,* Jun Jiang, Jizhen Li, Wuxi Xie, Xitong Zhao, Tao Guo, and Xuezhong Fan*

Cite This: *ACS Omega* 2022, 7, 25732−25740

Read Online

ACCESS | Metrics & More | Article Recommendations | Supporting Information

ABSTRACT: Four *N*,*N*-dimethylaminomethylferrocene polynitrogen catalysts were applied to the thermal decomposition of FOX-12, and their catalytic effect on FOX-12 was investigated by TG-DSC. The kinetic parameters and kinetic model of the mixed system were revealed by the Kissinger method, Freidman method, and combined kinetic analysis. The results showed that MAFcTAZ is the catalyst with the strongest effect on FOX-12, the decomposition peak temperature of FOX-12 is reduced, and the decomposition weight loss is higher than those for other catalysts, which prove that the decomposition of FOX-12 is more thorough under the catalysis of MAFcTAZ. The introduction of the four catalysts reduced the thermal decomposition peak temperature of FOX-12. MAFcTAZ was the most active catalyst for the decomposition of FOX-12, and the maximum heat release of catalyzing the decomposition of FOX-12 can reach 1236.76 J·g^{-1}. The activation energy (E_a) of FOX-12 decomposition decreased from 217.91 to 128.19, 137.85, 157.65, and 151.91 kJ·mol^{-1} under the effect of $MAFcNO_3$, MAFcPA, MAFcNTO, and MAFcTAZ. The Freidman analysis illustrated that MAFcTAZ reduced the activation energy during the entire decomposition process of FOX-12. The physical model of the decomposition reaction of FOX-12 transformed from the random nucleation and two-dimensional growth of nuclei model (A2) to the random scission model (L2) in the presence of $MAFcNO_3$ and two-dimensional diffusion (D2) under the effect of MAFcPA, MAFcNTO, and MAFcTAZ. By analyzing the molecular structures, MAFcTAZ has a higher iron content and nitrogen content, which are the essence of its excellent catalytic performance. From the perspective of interaction energy, the strong catalytic effect of MAFcTAZ is attributed to its large interaction energy with FOX-12 by energy decomposition analysis.

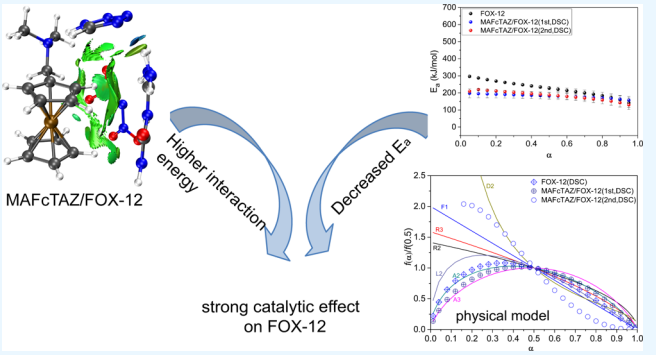

1. INTRODUCTION

By virtue of a lower sensitivity, non-hygroscopicity, and thermal stability, FOX-12 is considered to be a promising candidate for use in low sensitivity propellants and insensitive munition explosives.[1−3] Researchers have conducted preliminary evaluations on the combustion characteristics and energy performance of multicomponent propellants containing FOX-12. FOX-12 was applied to the composite modified double base propellant formulation, and the process safety of the propellant was evaluated: the actual formula showed a good combustion performance, and the pressure exponent met the requirements of engineering application.[4] The effect of FOX-12 content on the burning rate and sensitivity of propellant was investigated to reduce the sensitivity of high burning rate hydroxyl-terminated polybutadiene propellants. When the FOX-12 content is 5%, the maximum decrease in the propellant burning rate is 4.75% under 4−10 MPa, while the friction sensitivity decreased from 96 to 68%.[5] The combustion properties (burning rate and combustion flame structures) of propellants with a dual oxidizer (FOX-12 and ammonium dinitramide) were detected. The combustion flame structures at various pressures present a multiflame structure, and the brightness of flame increases with an increase in pressure.[6]

Thermal decomposition of energetic materials plays an important role in their practice application in propellants. The activation energy value of FOX-12 decomposition was 277 kJ·mol^{-1} measured with DSC; FOX-12 has a larger activation energy, indicating a high degree of thermal stability.[7] The kinetic parameters with a temperature-programmed mode were applied, and the E_a value of the exothermic decomposition reaction of FOX-12 is calculated to be 220.20 kJ·mol^{-1}.[8] These different results were attributed to the experimental conditions and processing methods employed.[9] The thermal decomposition mechanism of FOX-12 was elucidated by theoretical calculations coupled with online photoionization mass

Received: May 15, 2022
Accepted: June 29, 2022
Published: July 12, 2022

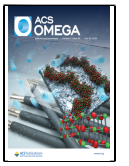

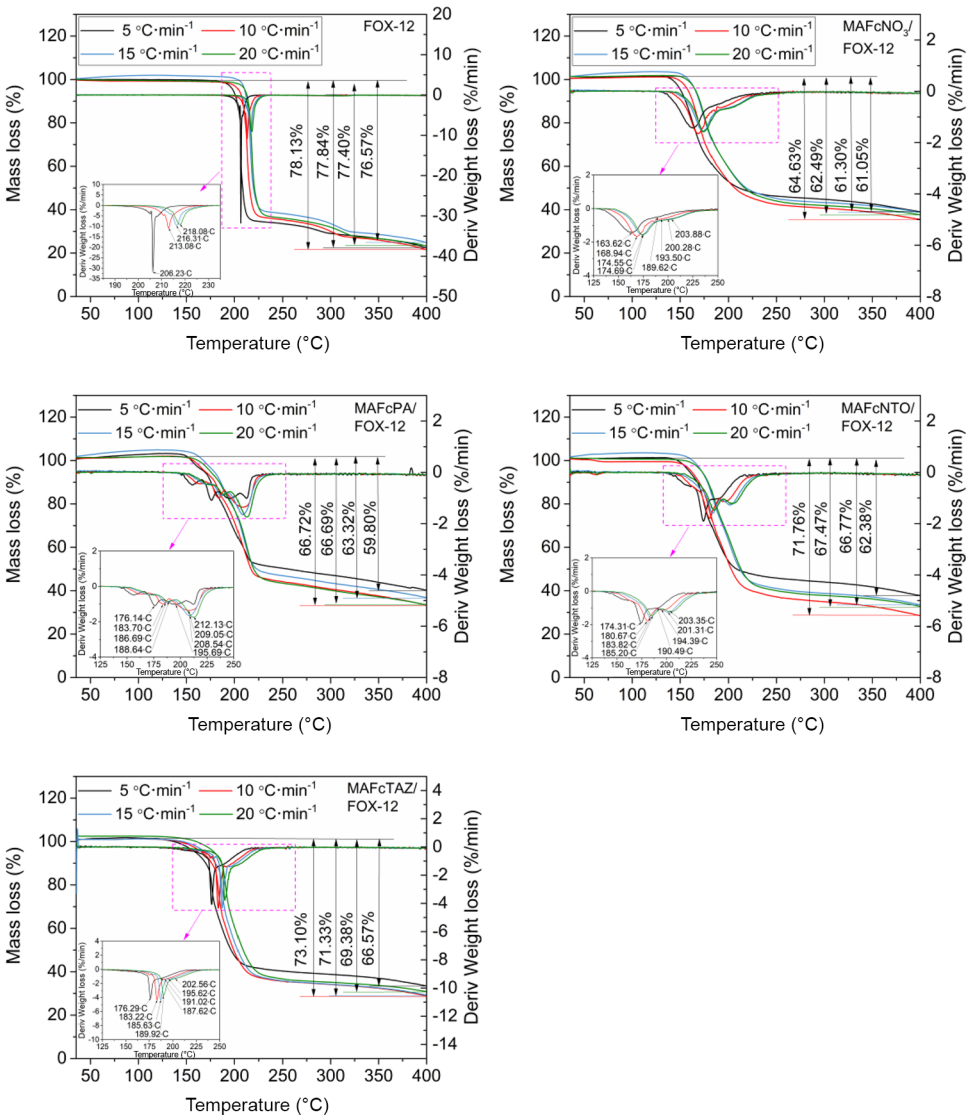

Figure 1. TG/DTG curves of FOX-12 decomposition with or without catalysts at various heating rates.

spectrometry and TG-DSC-IR-MS.[10] The thermal decomposition of FOX-12 itself has been extensively studied. The development of new weapon systems has different requirements for the burn rate of the composite solid propellant, and the regulation of the burning rate usually adopts the method of adding a burning rate catalyst to adjust the thermal decomposition performance of the oxidant, thereby affecting the burning rate. The catalysts that have been reported to promote the thermal decomposition of FOX-12 so far include the CuO/CNTs composite catalyst and SnO_2-Cu_2O/CNTs composite catalyst.[11,12] In order to promote the application of composite propellants containing FOX-12 and ammonium perchlorate (AP), it is necessary to find a catalyst that is effective for both AP and FOX-12 decomposition. As we all know, a ferrocene catalyst is a commonly used additive to boost the thermal decomposition of AP. If the addition of a ferrocene compound can catalyze the decomposition of FOX-12 at the same time, it will undoubtedly maximize the effectiveness of the catalyst.

In this work, four *N*,*N*-dimethylaminomethylferrocene energetic salts were prepared and the thermal decomposition of the mixture with FOX-12 was studied by a TG-DSC technique. The thermal decomposition kinetic parameters and kinetic models were analyzed with the Kissinger method, Friedman method, and combined kinetic analysis. The results from the kinetic analyses can provide more insights into the catalytic mechanism of the ferrocene catalyst for FOX-12 decomposition. Based on interaction region indicator (IRI) analysis and energy decomposition analysis on the basis of forcefield (EDA-FF), the weak interactions and interaction energies between FOX-12 and the different catalysts were analyzed in detail.

2. METHODS

2.1. Preparation of Catalyst Samples. Four ferrocene catalysts were prepared by the reaction between *N*,*N*-dimethylamino-methylferrocene and four energetic compounds, namely, 5-nitro-2,4-dihydro-3*H*-1,2,4-triazol-3-one (NTO), picric acid (PA), ammonium nitrate, and 1*H*-tetrazole. The preparation process of *N*,*N*-dimethylaminomethylferrocene nitrate ($MAFcNO_3$) was as follows: ammonium nitrate (2.16 g, 0.027 mmol) was dissolved in acetone and then an acetone solution of *N*,*N*-dimethylamino-methylferrocene (7.29 g, 0.03 mmol) was added under stirring. A yellow

https://doi.org/10.1021/acsomega.2c03026
ACS Omega 2022, 7, 25732−25740

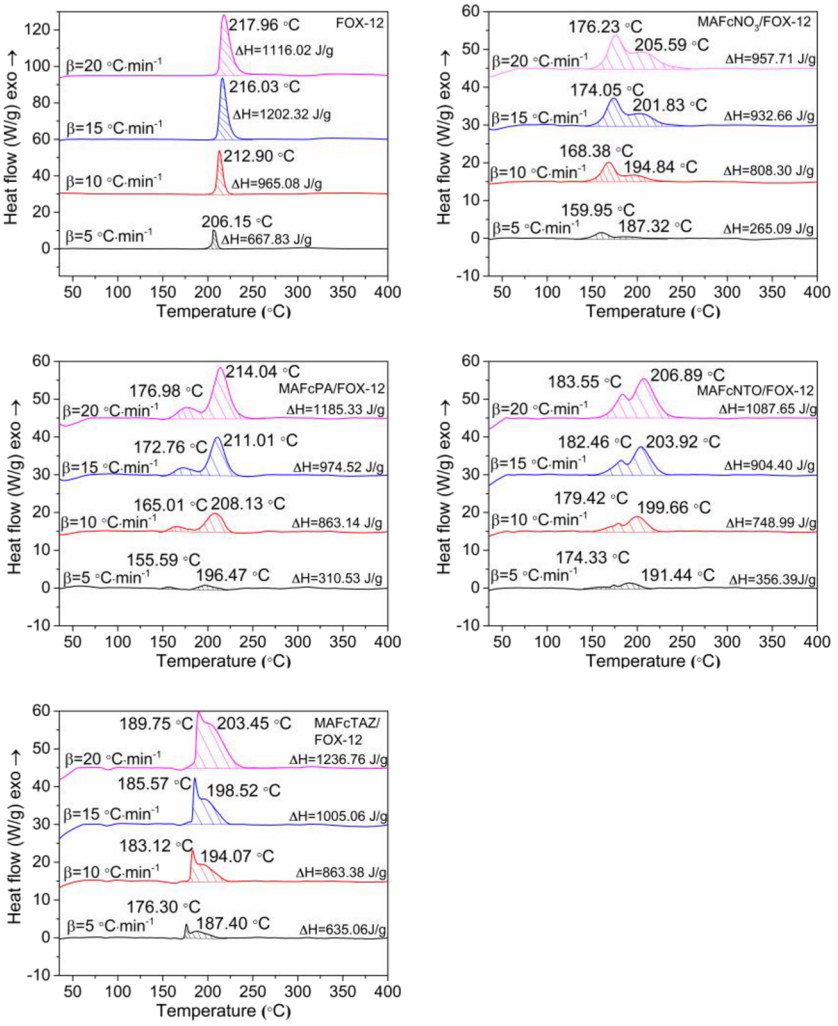

Figure 2. DSC curves for decomposition of FOX-12 with or without catalysts at various heating rates.

precipitate gradually formed, and the solution was stirred for another 2 h. The solid was collected by filtration and washed three times with diethyl ether. After drying it under vacuum for 24 h at 40 °C, $MAFcNO_3$ was obtained. The other three catalysts were prepared in the same way as $MAFcNO_3$, but the solvent used in the preparation of MAFcPA is methanol and the others use acetone. The details of the catalysts have been described before,[13] and thus the infrared spectra and ^1H NMR spectra were obtained to confirm the successful synthesis of the catalyst samples, as displayed in the Supporting Information.

2.2. Experiments. All catalysts were evenly mixed with FOX-12 in an agate mortar. The DSC experiments were performed on a Mettler TG-DSC instrument. The flow rate of argon was kept at 50 mL·min^{-1} during the experiment, and the samples were heated from 40 to 400 °C with a sample mass of about 1 mg. The heating rates were set as 5, 10, 15, and 20 °C·min^{-1}.

2.3. Thermal Decomposition Kinetics. The thermal decomposition kinetics of the different catalysts on FOX-12 decomposition were studied by using the nonisothermal TG and DSC data. In this work, the activation energy and pre-exponential factor were first determined by the Kissinger method.[14] With regard to the whole decomposition process to compare the results calculated with a single exothermic peak data, the widely used Freidman's isoconversional method and combined kinetics analysis were employed for revealing the dependence of activation energy on the conversion rate and the kinetic parameters and the physical model.[15,16]

2.4. Computational Details. The molecular structures of $MAFcNO_3$, MAFcPA, MAFcNTO, and MAFcTAZ were obtained from the Cambridge Structural Database at Cambridge Crystallographic Data Centre (CCDC number: 1485257, 1492192, 1485258, and 1491389).[17] The molecular configuration search of the mixture model of several catalysts was performed with a Molclus program;[18] the initial configurations (number of configurations: 50) were generated, and then an xtb program[19] through Molclus was used to perform batch optimization on each structure generated in the previous step to generate the optimized coordinates and energy of each structure. The isostat tool attached to Molclus was started, and the structure file obtained in the previous step was loaded. This tool will sort the structures according to their energy and make statistics to get the structure with the lowest energy. The structure with the lowest energy was used to generate the input file of the ORCA 4.2.1 program[20] in the Multiwfn program,[21] and then the geometry optimization using the PBE0-D3[22] method in combination with the def2-SV(P) basis set[23] was implemented in the ORCA program; the RIJCOSX technique was enabled for all the calculation.[24] Then, the wavefunction information was processed and

https://doi.org/10.1021/acsomega.2c03026
ACS Omega 2022, 7, 25732−25740

Table 1. Temperature Range for FOX-12 Mixed with or without Catalysts under Different Heating Rates

samples	stage	5 °C·min^{-1}	10 °C·min^{-1}	15 °C·min^{-1}	20 °C·min^{-1}
FOX-12		195.34−215.08	198.34−232.04	201.49−241.55	202.55−254.19
MAFcNO$_3$/FOX-12	1st	134.95−175.72	137.28−184.13	144.01−184.79	146.68−193.87
	2nd	175.72−231.65	184.13−230.23	184.79−253.53	193.87−261.61
MAFcPA/FOX-12	1st	147.18−177.88	148.92−186.29	151.67−190.70	152.67−193.37
	2nd	177.88−223.91	186.29−232.40	190.70−241.55	193.37−256.03
MAFcNTO/FOX-12	1st	142.51−179.13	150.26−185.63	151.17−189.62	153.33−191.78
	2nd	179.13−216.09	185.63−233.64	189.62−236.39	191.78−256.36
MAFcTAZ/FOX-12	1st	171.15−180.80	175.55−189.95	174.14−193.03	174.73−197.19
	2nd	180.80−215.17	189.95−226.57	193.03−227.04	197.19−247.04

calculated in the Multiwfn program to get the interaction region indicator (IRI) analysis and energy decomposition analysis based on forcefield;[25,26] the visualization images were drawn in the Visual Molecular Dynamics (VMD) software.[27]

3. RESULTS AND DISCUSSION

3.1. Mass Loss Properties. To study the effect of ferrocenyl-based catalysts on the thermal stability of FOX-12, the TG/DTG curves of FOX-12 with or without catalysts are displayed in Figure 1. It can be clearly seen that the decomposition of FOX-12 undergoes a rapid mass loss and a slow mass loss. Thermogravimetric measurements gave peaks of 206.23, 213.08, 216.31, and 218.08 °C at heating rates of 5, 10, 15, and 20 °C min^{-1}, respectively. The higher the heating rate, the more obvious the thermal hysteresis. TG analysis of pure FOX-12 shows mass losses of 77.84, 78.13, 76.57, and 77.40% in the decomposition process from 40 to 400 °C, resulting in the residues of 22.16, 21.87, 22.60, and 23.43% at different heating rates. Under the effect of MAFcNO$_3$, the decomposition of the mixture of MAFcNO$_3$ and FOX-12 shows two broader exothermic peaks: the first exotherm corresponds to the catalyst decomposition, resulting in a mass loss of 33.13−36.40%, and the second exotherm is attributed to the FOX-12 decomposition. The decomposition peak temperatures are reduced by 18.61−22.06 °C compared with pure FOX-12, and the mass loss yield is 61.05−64.63%. The mass loss of MAFcPA in the first decomposition stage is 17.41−17.79%, and the peak temperatures of FOX-12 are decreased by 4.05−10.54 °C, resulting in a mass loss of 59.80−66.72%. For the MAFcNTO/FOX-12 mixture, the catalyst decomposes and the mass loss is 28.38−33.12%. The decomposition peak temperatures of FOX-12 are reduced to 190.49, 194.39, 201.31, and 203.35 °C. Therefore, MAFcNTO reduces the decomposition peak temperature of FOX-12 by about 15 °C. The weight losses of MAFcNTO/FOX-12 are 62.38, 71.76, 66.77, and 67.47%. In comparison, these weight losses are larger than those under the effect of the first two catalysts (MAFcNO$_3$ and MAFcPA). MAFcTAZ has the strongest catalytic effect on FOX-12 decomposition, and it loses 32.20−36.50% of its mass in the first stage, and the peak temperatures of FOX-12 are decreased by 15.52−22.06 °C, resulting in a mass loss of 66.57−73.10%. In conclusion, the order of the magnitude of the mass loss for the four catalysts in the first stage is MAFcTAZ > MAFcNO$_3$ > MAFcNTO > MAFcPA, and the order in which the four catalysts reduce the decomposition peak temperature of FOX-12 is MAFcTAZ > MAFcNO$_3$ > MAFcNTO > MAFcPA, indicating that the more thorough the decomposition of the catalyst, the stronger the catalytic effect on FOX-12.

3.2. Heat Release Properties. The thermal decomposition behavior can be visually assessed by DSC curves. Figure 2 shows the DSC curves for FOX-12 decomposition with or without catalysts at various heating rates. Through careful analysis on DSC graphs, it was found that the decomposition of FOX-12 in the second stage showed a sharp peak or a blunt peak depending on the decomposition of the catalysts. When the heat release of the catalyst in the first stage is greater than the heat release of FOX-12 in the second stage, the decomposition of FOX-12 shows a blunt peak, otherwise it shows a sharp peak. In addition, for MAFcTAZ/FOX-12, since the heat release of MAFcTAZ is larger than the FOX-12 decomposition and the decomposition peak temperature of MAFcTAZ is between 176.30 and 189.75 °C, the decomposition peak of the first stage is much closer to the decomposition peak of FOX-12, and thus a shoulder-like peak appears. For pure FOX-12, the peak temperatures are 206.15, 212.90, 216.03, and 217.96 °C at heating rates of 5, 10, 15, and 20 °C min^{-1}. The peak temperature at 212.90 °C is consistent with the literature data reported by Ostmark et al.[7] When the heating rate increases, the energy release also enhances. FOX-12 displays a heat release of 1202.32 J·g^{-1} at 15 °C·min^{-1}. In the presence of MAFcNO$_3$, the decomposition of the mixture of MAFcNO$_3$ and FOX-12 shows two broader exothermic peaks. The effect of MAFcNO$_3$ on FOX-12 is that the exothermic peak temperatures were decreased by 18.83, 18.06, 14.2, and 12.37 °C at various heating rates, and the heat release did not increase. The effect of MAFcPA on FOX-12 is similar to that of MAFcNO$_3$. Compared to FOX-12, the exothermic peak temperatures are reduced by 9.68, 4.77, 5.02, and 3.92 °C, respectively. The heat release is lower than pure FOX-12 but higher than MAFcNO$_3$ and FOX-12, and the maximum heat release can reach 1185.33 J·g^{-1}. The addition of MAFcNTO reduced the exothermic peak temperatures by 15.21, 13.23, 12.11, and 10.20 °C, and the maximum heat release is 1087.65 J·g^{-1}. Among the four catalysts, MAFcTAZ is an excellent catalyst with a maximum heat release of 1236.76 J·g^{-1}. At the same time, it can be calculated that the reduction of peak temperature in the presence of MAFcTAZ is the greatest. From the heat release data, the DSC graphs show that the heat release of pure FOX-12 is slightly larger than catalyzed FOX-12, which may be due to the heat release by the catalytic decomposition reaction that accumulates in the gas phase, resulting in a lower exothermic heat measured by the instrument.[28]

3.3. Thermal Decomposition Kinetics. *3.3.1. Kinetics Parameters Calculated by the Kissinger Method.* Under the effect of the four ferrocenyl catalysts, the thermal decomposition of the mixed system can be divided into two stages. The decomposition temperature range of the two stages of

https://doi.org/10.1021/acsomega.2c03026
ACS Omega 2022, 7, 25732−25740

Table 2. Comparison of the Kinetic Parameters Obtained by the Kissinger Method for FOX-12 Mixed with or without Catalysts

		TGA			DSC		
samples	stage	E_k (kJ·mol^{-1})	log A (s^{-1})	r	E_k (kJ·mol^{-1})	log A (s^{-1})	r
FOX-12		222.08	18.23	0.9897	217.91	17.78	0.9960
MAFcNO$_3$/FOX-12	1st	174.14	14.96	0.9787	125.96	9.32	0.9966
	2nd	158.48	11.98	0.9695	128.19	8.64	0.9952
MAFcPA/FOX-12	1st	179.52	14.95	0.9921	94.88	5.71	0.9977
	2nd	137.42	9.36	0.9271	137.85	9.37	0.9807
MAFcNTO/FOX-12	1st	202.38	17.72	0.9934	238.47	21.93	0.9900
	2nd	171.82	13.48	0.9717	157.65	11.79	0.9979
MAFcTAZ/FOX-12	1st	173.20	14.23	0.9921	175.46	14.50	0.9927
	2nd	151.70	11.37	0.9350	151.91	11.33	0.9930

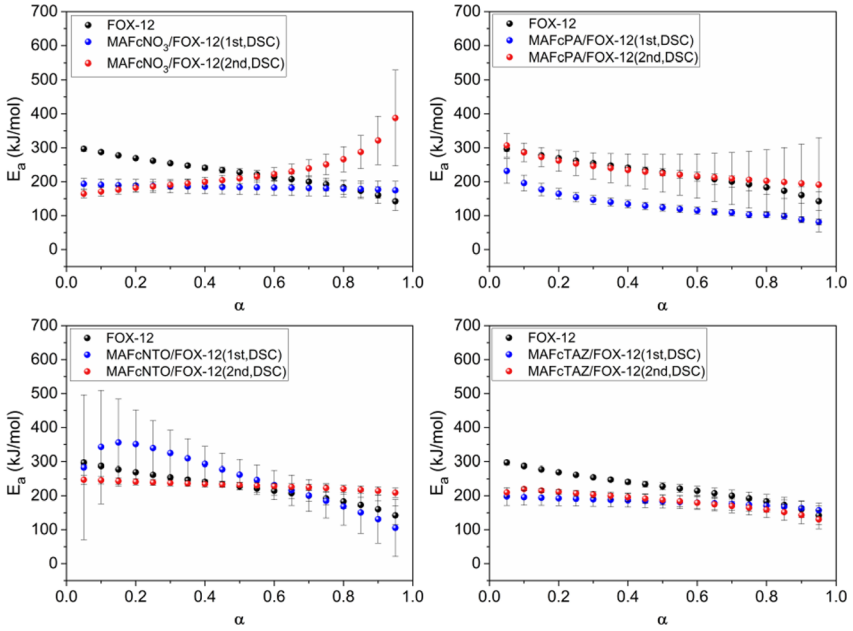

Figure 3. E_a–α curves of the thermal decomposition of FOX-12 with or without catalysts.

Table 3. Parameters for the Decomposition Reaction Models of FOX-12 with or without Catalysts Evaluated from DSC Data

		combined kinetic method				Friedman method		Kissinger method	
samples	stage	m	n	$E_{a(1)}$	cA/min^{-1}	$E_{a(2)}$	r	$E_{a(3)}$	log A
FOX-12		0.614	1.134	205.22 ± 4.05	8.51 ± 8.5 × 10^{21}	220.47	0.9959	217.91	17.78
MAFcNO$_3$/FOX-12	1st	0.191	0.985	185.41 ± 2.61	1.07 ± 0.7 × 10^{21}	183.13	0.9861	125.96	9.32
	2nd	0.588	1.463	232.32 ± 6.41	5.40 ± 8.8 × 10^{24}	220.41	0.9908	128.19	8.64
MAFcPA/FOX-12	1st	0.420	1.277	111.71 ± 1.91	1.12 ± 0.5 × 10^{12}	121.18	0.9926	94.88	5.71
	2nd	−0.221	1.535	239.29 ± 8.86	1.49 ± 3.3 × 10^{25}	222.18	0.9234	137.85	9.37
MAFcNTO/FOX-12	1st	−0.060	0.863	262.44 ± 11.2	1.01 ± 3.1 × 10^{29}	246.96	0.9572	238.47	21.93
	2nd	0.162	1.623	226.47 ± 1.14	1.41 ± 0.4 × 10^{24}	229.72	0.9985	157.65	11.79
MAFcTAZ/FOX-12	1st	0.708	0.946	177.35 ± 2.82	5.34 ± 3.9 × 10^{19}	181.06	0.9885	175.46	14.50
	2nd	0.471	2.407	172.56 ± 2.97	3.64 ± 2.7 × 10^{18}	182.74	0.9907	151.91	11.33

different mixed systems was divided and is listed in Table 1. After that, the thermal decomposition kinetic parameters were calculated for the two stages, as shown in Table 2. By using the Kissinger method, the apparent activation energy and pre-exponential factor of FOX-12 processed by DTG data and DSC data are 222.08 kJ·mol^{-1} with a log A of 18.23 s^{-1} and 217.91 kJ·mol^{-1} with a log A of 17.78 s^{-1}; these E_a values are close to the reported results.[8] For the mixture system, the first decomposition stage corresponds to the catalyst decomposition and the second decomposition stage is the decomposition of FOX-12 under the effect of the catalysts. The E_a values of MAFcNO$_3$, MAFcPA, MAFcNTO, and MAFcTAZ are calculated to be 125.96, 94.88, 238.47, and 175.46 kJ·mol^{-1}, respectively. Under the different catalysts, the E_a values of FOX-12 decreased by 89.72, 80.06, 60.26, and 66.00 kJ·mol^{-1}, which indicated that all catalysts can reduce the activation energy of FOX-12 decomposition.

3.3.2. Dependence of Activation Energy on the Conversion Rate. The Kissinger method is based on peak temperature data and does not account for changes in the

https://doi.org/10.1021/acsomega.2c03026
ACS Omega 2022, 7, 25732−25740

overall process. By using the Freidman method, the E_a was calculated by DSC data and the dependence of E_a on the conversion rate (α) is presented in Figure 3. The average E_a value of FOX-12 is 220.47 kJ·mol^{-1} obtained by Friedman analysis when α is in the range of 0.3−0.8. The effect mechanism of $MAFcNO_3$ on FOX-12 can be summarized as reducing the activation energy of FOX-12 decomposition before the conversion reached 0.6. MAFcPA has no noticeable impact on the activation energy of FOX-12 decomposition. For MAFcNTO, the activation energy of FOX-12 decomposition is reduced before the conversion reached 0.4. The E_a of FOX-12 is decreased in the presence of MAFcTAZ, its excellent catalytic performance can be attributed to its lower activation energy, and the catalyst has the highest activity, thus reducing the activation energy during the entire decomposition process of FOX-12.

The kinetic parameters calculated by the Kissinger method, Freidman method, and combined kinetic analysis are listed in Table 3. It can be seen that different methods yield slightly different results. From the results of the average activation energy obtained by the Friedman method, the E_a of FOX-12 decomposition changed from 220.47 to 220.41, 222.18, 229.72, and 182.74 kJ·mol^{-1} in the presence of $MAFcNO_3$, MAFcPA, MAFcNTO, and MAFcTAZ, respectively, indicating that the addition of MAFcTAZ can reduce the activation energy of FOX-12 decomposition, while $MAFcNO_3$, MAFcPA, and MAFcNTO have little effect on the activation energy of FOX-12 decomposition. The E_a of FOX-12 obtained by CKA analysis dropped from 205.22 to 172.56 kJ·mol^{-1}, and thus MAFcTAZ is the most active catalyst for FOX-12.

3.4. Physical Model. The combined kinetic analysis implies a simultaneous analysis of experimental data for the solid-state reaction obtained under any experimental conditions.[29] Table 4 shows the functions corresponding to the most commonly used mechanisms reported in the literature;[30] the difference of kinetic models lies in the driving force, i.e., interface growth, diffusion, and nucleation growth. The fitting function for $f(\alpha)$ was drawn like an umbrella that covers any of the kinetic functions that would describe a solid-state reaction. When analyzing real data, the normalized curve obtained from the experiment is more consistent with one ideal model curve, indicating that the thermal decomposition follows this kinetic model. As shown in Figure 4, it can be readily seen that the FOX-12 decomposition follows the random nucleation and two-dimensional growth of nuclei model (A2). The $MAFcNO_3$ decomposition is controlled by a phase boundary controlled reaction (R3). When adding $MAFcNO_3$ into FOX-12, the FOX-12 decomposition changes into a random scission model (L2). Under the effect of MAFcPA, FOX-12 follows a two-dimensional diffusion model (D2), and the decomposition reaction of MAFcPA is dominated by the L2 model. The MAFcNTO decomposition is controlled by the F1 model, and the thermal decomposition of the MAFcNTO-FOX-12 system follows a first-order reaction (D2). The physical model of MAFcTAZ is assigned to the random nucleation and three-dimensional growth of nuclei model (A3), and FOX-12 decomposition transferred from the A2 model to D2 model. Therefore, the addition of several ferrocene catalysts changed the physical model of FOX-12 decomposition, and in combination with DSC and kinetic parameters, the two-dimensional diffusion model makes the catalytic reactions more vigorous.

Table 4. Kinetic Functions for the Most Widely Used Kinetic Models

mechanism	symbol	$f(\alpha)$
phase boundary controlled reaction (contracting area)	R2	$(1-\alpha)^{1/2}$
phase boundary controlled reaction (contracting volume)	R3	$(1-\alpha)^{2/3}$
unimolecular decay law (instantaneous nucleation and unidimensional growth)	F1	$(1-\alpha)$
random instant nucleation and two-dimensional growth of nuclei (Avrami−Erofeev equation)	A2	$2(1-\alpha)[-\ln(1-\alpha)]^{1/2}$
random instant nucleation and three-dimensional growth of nuclei (Avrami−Erofeev equation)	A3	$3(1-\alpha)[-\ln(1-\alpha)]^{2/3}$
two-dimensional diffusion (bidimensional particle shape)	D2	$1/[-\ln(1-\alpha)]$
random scission model	L2	$2(\alpha^{1/2}-\alpha)$

3.5. Catalytic Mechanism. According to the DSC data of the mixed system of the different catalysts and FOX-12, it can be seen that the catalysts have an influence on the decomposition peak temperature of FOX-12. The more the catalyst reduces the decomposition peak temperature of FOX-12, the better the catalytic performance of FOX-12. For the different catalysts, the order of catalytic performance is MAFcTAZ > $MAFcNO_3$ > MAFcNTO > MAFcPA based on peak temperature results. It is recognized by researchers that the Fe content in the molecular structure of ferrocene derivatives is positively related to its catalytic performance at a certain extent.[31] Thus, we analyzed the element distribution of the different catalysts synthesized, as shown in Figure 5. $MAFcNO_3$ has a higher Fe content, and MAFcTAZ has a stronger catalytic effect on FOX-12 decomposition, which can be attributed to the Fe content dominating the catalytic effect, but the nitrogen content in the molecule also has a certain influence on the catalytic performance.

The interaction region indicator (IRI) can intuitively show the chemical bonds and weak interactions in the chemical system. The IRI = 1.0 isosurface maps were drawn to reveal the interaction between the catalysts and FOX-12. For the convenience of analysis, only the intermolecular interactions are shown in Figure 6. There is a van der Waals interaction between $MAFcNO_3$ and FOX-12, and a weak hydrogen bond attraction between the nitrate group in the $MAFcNO_3$ molecule and the amino group on FOX-12. In the MAFcPA and FOX-12 system, the van der Waals effect is relatively concentrated between the picrate ion and FOX-12. The van der Waals interaction between MAFcNTO and FOX-12 is distributed between the FOX-12 molecule and the cyclopentadiene ring, and there is a weak attraction between the NTO molecule and the *N*-guanylurea group. The interaction region of MAFcTAZ and FOX-12 is located in the FOX-12 molecule and ferrocene group. Furthermore, energy decomposition analysis based on forcefield (EDA-FF) is a convenient method that can not only replace the more expensive energy decomposition methods based on wave functions but also has some unique advantages, such as visualization of interaction regions and convenient investigation of weak interactions. The EDA-FF method was applied to investigate intermolecular weak interactions, the magnitude of interaction energies, and the interaction components.[26,32,33] The interaction energies between FOX-12 and the different catalysts were obtained by energy decomposition analysis based on forcefield, as listed in Table 5. The interaction energies for FOX-12 with $MAFcNO_3$, MAFcPA, MAFcNTO, and MAFcTAZ are calculated to be

https://doi.org/10.1021/acsomega.2c03026
ACS Omega 2022, 7, 25732−25740

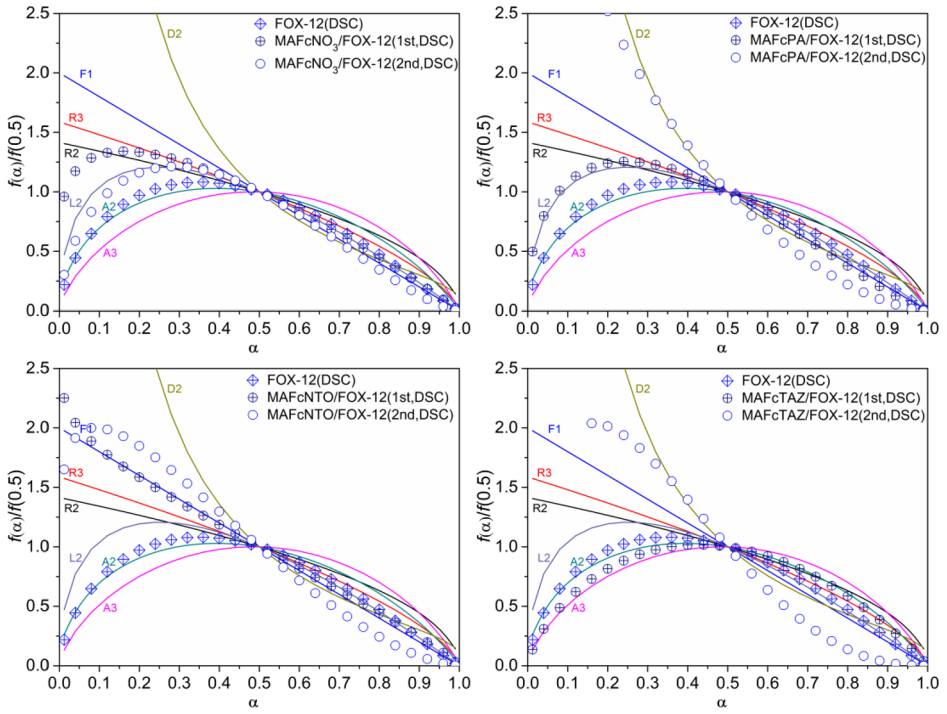

Figure 4. Comparison of normalized curves of obtained kinetic models for FOX-12 with and without catalysts by the combined kinetic analysis method. Notes: D2: two-dimensional diffusion; R2 and R3: phase boundary controlled reactions (contracting area and contracting volume, respectively); F1, first-order reaction; A2 and A3: random nucleation and two- and three-dimensional growth of nuclei; and L2, random scission model.

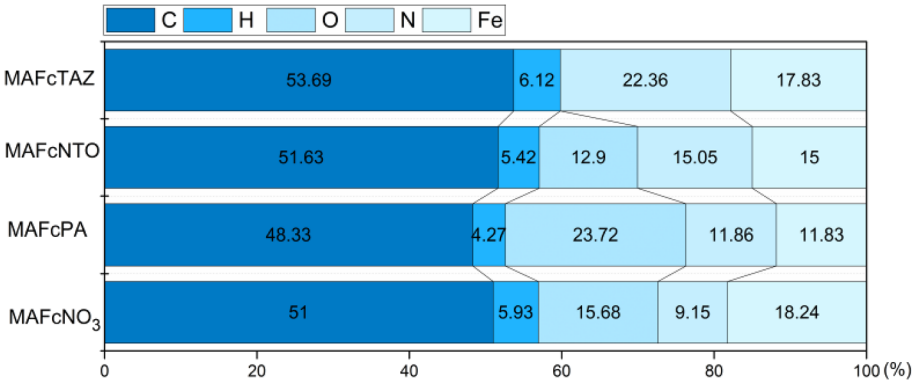

Figure 5. Element distribution of $MAFcNO_3$, MAFcPA, MAFcNTO, and MAFcTAZ.

−232.97, −169.84, −114.30, and −222.29 kJ·mol^{-1}, respectively, and the interaction energy between MAFcTAZ and FOX-12 is greater than those between MAFcPA, MAFcNTO, and FOX-12. Therefore, the strong catalytic effect of MAFcTAZ is attributed to its large interaction energy with FOX-12.

4. CONCLUSIONS

The effect of the four ferrocenyl catalysts on the thermal decomposition of FOX-12 was studied by the TG-DSC technique, and the kinetics parameters were analyzed by the Kissinger method, Freidman method, and combined kinetics analysis. The conclusions are as follows:

(1) TG data showed that the higher the heating rate, the more obvious the thermal hysteresis. For the mixture system of FOX-12 and the different catalysts, FOX-12 decomposes in advance, and the amount of residue also increases accordingly. MAFcTAZ is the catalyst with the strongest effect on FOX-12, and its decomposition weight losses are 66.57, 73.10, 71.33, and 69.38%, respectively, which proves that under the catalysis of MAFcTAZ, the decomposition of FOX-12 is more thorough.

(2) By using the Kissinger method, the apparent activation energy and pre-exponential factor processed by DSC data are 217.91 kJ·mol^{-1} with a log A of 17.78 s^{-1}. For the mixture system, under the effect of $MAFcNO_3$, MAFcPA, MAFcNTO, and MAFcTAZ, the E_a of FOX-12 decreased by 89.72, 80.06, 60.26, and 66.00 kJ·mol^{-1}, respectively, which indicated that all catalysts can reduce the activation energy of FOX-12 decomposition.

(3) The kinetic parameters obtained by CKA analysis suggested that the E_a of FOX-12 decomposition dropped from 205.22 to 172.56 kJ·mol^{-1}, and thus MAFcTAZ is the most active catalyst for FOX-12. The decomposition

https://doi.org/10.1021/acsomega.2c03026
ACS Omega 2022, 7, 25732−25740

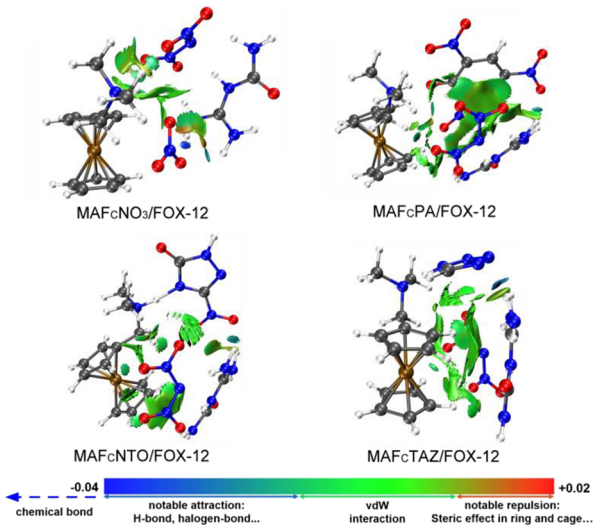

Figure 6. IRI = 1.0 isosurface maps of FOX-12 with different catalysts.

Table 5. Interaction Components of FOX-12 with Different Catalysts by Energy Decomposition Analysis Based on Forcefield

	interaction energy (kJ·mol^{-1})			
samples	electrostatic	exchange-repulsion	dispersion	total
MAFcNO$_3$/FOX-12	−219.83	83.22	−96.35	−232.97
MAFcPA/FOX-12	−110.25	110.62	−170.20	−169.84
MAFcNTO/FOX-12	−80.65	84.60	−118.35	−114.30
MAFcTAZ/FOX-12	−227.13	96.91	−92.70	−222.29

reaction of FOX-12 follows the random scission model (L2) in the presence of MAFcNO$_3$ and two-dimensional diffusion (D2) under the effect of MAFcPA, MAFcNTO, and MAFcTAZ.

(4) The reason for the high catalytic activity of MAFcTAZ is that the high Fe content in the molecular structure plays a leading role and the nitrogen content also has a certain influence on the catalytic performance. From the perspective of interaction energy, the strong catalytic effect of MAFcTAZ is attributed to its large interaction energy with FOX-12.

■ ASSOCIATED CONTENT

Supporting Information

The Supporting Information is available free of charge at https://pubs.acs.org/doi/10.1021/acsomega.2c03026.

Details of IR and ^{1}H NMR spectra of the four ferrocenyl catalysts (PDF)

■ AUTHOR INFORMATION

Corresponding Authors

Xiaolong Fu − *Xi'an Modern Chemistry Research Institute, Xi'an 710065, China*; Email: fuxiaolong204@163.com

Xuezhong Fan − *Xi'an Modern Chemistry Research Institute, Xi'an 710065, China*; Email: xuezhongfan@126.com

Authors

Liping Jiang − *Xi'an Modern Chemistry Research Institute, Xi'an 710065, China*; orcid.org/0000-0003-4045-0770

Jun Jiang − *Xi'an Modern Chemistry Research Institute, Xi'an 710065, China*

Jizhen Li − *Xi'an Modern Chemistry Research Institute, Xi'an 710065, China*

Wuxi Xie − *Xi'an Modern Chemistry Research Institute, Xi'an 710065, China*

Xitong Zhao − *Xi'an Modern Chemistry Research Institute, Xi'an 710065, China*; orcid.org/0000-0002-5342-4638

Tao Guo − *Xi'an Modern Chemistry Research Institute, Xi'an 710065, China*

Complete contact information is available at: https://pubs.acs.org/10.1021/acsomega.2c03026

Notes

The authors declare no competing financial interest.

■ ACKNOWLEDGMENTS

This work was financially supported by the National Natural Science Foundation of China (21975150).

■ REFERENCES

(1) Badgujar, D.; Talawar, M. Thermal Analysis and Sensitivity Studies on Guanylurea Dinitramide (GUDN or FOX-12) Based Melt Cast Explosive Formulations. *Cent. Eur. J. Energ. Mater.* **2017**, *14*, 296−303.

(2) Kempa, P. B.; Herrmann, M.; Fuhr, I.; Oestmark, H. Crystal Structure and Thermal Expansion of FOX-12. *Int. Annu. Conf. ICT* **2009**, *58*, 40/1−40/11.

(3) Lei, Y. P.; Yang, S. Q.; Xu, S. L.; Zhang, T. Progress in Insensitive High Energetic Materials N-Guanylurea-Dinitramide. *Chin. J. Energ. Mater.* **2007**, *15*, 289−293.

(4) Pang, J.; Wang, J.; Zhang, R.; Xie, B. Application of CL-20, FOX-12 and DNTF in CMDB Propellant. *Chin. J. Explos. Propellants* **2005**, *28*, 19−21.

(5) Xu, H. X.; Zhao, F. Q.; Pang, W. Q.; Li, Y. H.; Yang, J.; Liu, Z. R. Properties of High Burning Rate HTPB Propellant Containing FOX-12. *J. Solid Rock Technol.* **2011**, *34*, 745−749.

(6) Pang, W. Q.; Wang, K.; Xu, H. X.; Li, J. Q.; Xiao, L. Q.; Fan, X. Z.; Li, H. Combustion Features of Nitrate Ester Plasticized Polyether Solid Propellants with ADN and FOX-12 Particles. *Int. J. Energ. Mater. Chem. Propul.* **2020**, *19*, 11−23.

(7) Ostmark, H.; Bemm, U.; Bergman, H.; Langlet, A. N-Guanylurea-Dinitramide: A New Energetic Material with Low Sensitivity for Propellants and Explosives Applications. *Thermochim. Acta* **2002**, *384*, 253−259.

(8) Zhao, F. Q.; Chen, P.; Yuan, H. A.; Gao, S. L.; Hu, R. Z.; Shi, Q. Z. Thermochemical Properties and Non-Isothermal Decomposition Reaction Kinetics of N-Guanylurea Dinitramide (GUDN). *Chin. J. Chem.* **2004**, *22*, 136−141.

(9) Santhosh, G.; Soumyamol, P. B.; Sreejith, M.; Reshmi, S. Isoconversional Approach for the Non-Isothermal Decomposition Kinetics of Guanylurea Dinitramide (GUDN). *Thermochim. Acta* **2016**, *632*, 46−51.

(10) Jiang, L. P.; Fu, X. L.; Fan, X. Z.; Li, J. Z.; Xie, W. X.; Zhang, G. F.; Zhou, Z. Y.; Zhang, W. Study on N-guanylurea-dinitramide (GUDN) Decomposition Using Theoretical Simulations, Online Photoionization Mass Spectrometry and TG-DSC-IR-MS Experiments. *Combust. Flame* **2021**, *229*, No. 111406.

(11) Liu, X.; Hong, W. L.; Zhao, F. Q.; Tian, D. Y.; Zhang, J. X.; Li, Q. S. Synthesis of CuO/CNTs Composites and Its Catalysis on Thermal Decomposition of FOX-12. *J. Solid Rock Technol.* **2008**, *31*, 508−511.

(12) Zhang, J.; Hong, W.; Zhao, F.; Liu, J.; Tian, D.; Zhu, X.; Ma, Y. Synthesis of SnO_2-Cu_2O/CNTs Catalyst and Its Catalytic Effect on Thermal Decomposition of FOX-12. *Chin. J. Explos. Propellants* **2011**, *34*, 47−51.
(13) Li, T.; Li, D. D.; Li, J. Z.; Zhang, G. F.; Zhang, W. Q.; Gao, Z. W. ″One-Step″ Synthesis of Ionic Ferrocenyl Compounds of Ferrocenylmethyldimethylamine. Characterization, Migration, and Catalytic Properties During Combustion. *Z. Anorg. Allg. Chem.* **2016**, *642*, 1095−1103.
(14) Kissinger, H. E. Reaction Kinetics in Differential Thermal Analysis. *Anal. Chem.* **1957**, *29*, 1702−1706.
(15) He, W.; Guo, J. H.; Cao, C. K.; Liu, X. K.; Lv, J. Y.; Chen, S. W.; Liu, P. J.; Yan, Q. L. Catalytic Reactivity of Graphene Oxide Stabilized Transition Metal Complexes of Triaminoguanidine on Thermolysis of RDX. *J. Phys. Chem. C* **2018**, *122*, 14714−14724.
(16) Chen, S. W.; He, W.; Luo, C. J.; An, T.; Chen, J.; Yang, Y. J.; Liu, P. J.; Yan, Q. L. Thermal Behavior of Graphene Oxide and Its Stabilization Effects on Transition Metal Complexes of Triaminoguanidine. *J. Hazard. Mater.* **2019**, *368*, 404−411.
(17) The Cambridge Crystallographic Data Centre (CCDC number: 1485257, 1492192, 1485258 and 1491389) Experimental Crystal Structure Determination, 2016, DOI: DOI: 10.5517/ccdc.csd.cc1lvjjh.
(18) Lu, T. *Molclus program*, Version 1.9.9.9, http://www.keinsci.com/research/molclus.html.
(19) Lu, T. gau_xtb: A Gaussian interface for xtb code, http://sobereva.com/soft/gau_xtb.
(20) Neese, F. Software Update: The Orca Program System, Version 4.0. *Wiley Interdiscip. Rev.: Comput. Mol. Sci.* **2018**, *8*, 1327.
(21) Lu, T.; Chen, F. W. Multiwfn: A Multifunctional Wavefunction Analyzer. *J. Comput. Chem.* **2012**, *33*, 580−592.
(22) Adamo, C.; Barone, V. Toward Reliable Density Functional Methods without Adjustable Parameters: The PBE0 Model. *J. Chem. Phys.* **1999**, *110*, 6158−6170.
(23) Schaefer, A.; Huber, C.; Ahlrichs, R. Fully Optimized Contracted Gaussian Basis Sets for Atoms Li to Kr. *J. Chem. Phys.* **1994**, *100*, 2571−2577.
(24) Kossmann, S.; Neese, F. Comparison of Two Efficient Approximate Hartee-Fock Approaches. *Chem. Phys. Lett.* **2009**, *481*, 240−243.
(25) Lu, T.; Chen, Q. Interaction Region Indicator (Iri): A Very Simple Real Space Function Clearly Revealing Both Chemical Bonds and Weak Interactions. *Chemistry—Methods* **2021**, *1*, 231−239.
(26) Lu, T.; Liu, Z. Y.; Chen, Q. X. Comment on "18 and 12−Member Carbon Rings (cyclo[n]carbons)−A Density Functional Study.". *Mater. Sci. Eng., B* **2021**, *273*, No. 115425.
(27) Humphrey, W.; Dalke, A.; Schulten, K. VMD: Visual Molecular Dynamics. *J. Mol. Graph* **1996**, *14*, 33−38.
(28) Hu, S. Q.; Kang, B.; Zhang, Y.; Liu, L. L.; Che, Q. M.; Liu, Y. M. Effect of Ferrocene Derivatives on the Thermal Decomposition of HAN/PVA. *Chin. J. Explo. Propell.* **2020**, *43*, 149−154.
(29) Perez-Maqueda, L. A.; Criado, J. M.; Sanchez-Jimenez, P. E. Combined Kinetic Analysis of Solid-state Reactions: A Powerful Tool for the Simultaneous Determination of Kinetic Parameters and the Kinetic Model without Previous Assumptions on the Reaction Mechanism. *J. Phys. Chem. A* **2006**, *110*, 12456−12462.
(30) Sánchez-Jiménez, P. E.; Pérez-Maqueda, L. A.; Perejón, A.; Criado, J. M. A New Model for the Kinetic Analysis of Thermal Degradation of Polymers driven by random scission. *Polym. Degrad. Stab.* **2010**, *95*, 733−739.
(31) Saravanakumar, D.; Sengottuvelan, N.; Narayanan, V.; Kandaswamy, M.; Varghese, T. L. Burning-Rate Enhancement of a High-Energy Rocket Composite Solid Propellant Based on Ferrocene-Grafted Hydroxyl-Terminated Polybutadiene Binder. *J. Appl. Polym.Sci.* **2011**, *119*, 2517−2524.
(32) Zhu, S. F.; Gan, Q.; Feng, C. G. Multimolecular Complexes of CL-20 with Nitropyrazole Derivatives:Geometric, Electronic Structure, and Stability. *ACS Omega* **2019**, *4*, 13408−13417.
(33) Chen, X.; Sakurai, H.; Wang, H.; Gao, S. M.; Bi, H. D.; Bai, F. Q. Theoretical Study on the Molecular Stacking Interactions and Charge Transport Properties of Triazasumanene Crystals − from Explanation to Prediction. *Phys. Chem. Chem. Phys.* **2021**, *23*, 4681−4689.

https://doi.org/10.1021/acsomega.2c03026
ACS Omega 2022, 7, 25732−25740